Gas-Phase Acidities of Tetrahedral Oxyacids from ab Initio Electronic Structure Theory

James R. Rustad,*,† David A. Dixon,*,† James D. Kubicki,‡ and Andrew R. Felmy†

Wiley Lab, Pacific Northwest National Laboratory, Richland, Washington 99352, and Department of Geosciences, 503 Deike Building, Pennsylvania State University, University Park, Pennsylvania 16802

Received: September 24, 1999; In Final Form: January 25, 2000

Density functional calculations have been performed on several protonation states of the oxyacids of Si, P, V, As, Cr, and S. Structures and vibrational frequencies are in good agreement with experimental values where these are available. A reasonably well-defined correlation between the calculated gas-phase acidities and the measured pK_a in aqueous solution has been found. The pK_a/gas-phase acidity slopes are consistent with those derived from previous molecular mechanics calculations on ferric hydrolysis and the first two acidity constants for orthosilicic acid. The successive deprotonation of other H_nTO_4 species, for a given tetrahedral anion T are roughly consistent with this slope, but not to the extent that there is a universal correlation among all species.

I. Introduction

Because of their negative charge and generally high solubility, oxyanions of transition metals and other elements form a class of compounds that can be highly mobile in groundwater systems.[1,2] The chemical behavior of oxyanions is important in a number of environmental waste disposal areas including U.S. Department of Energy (DOE) sites,[3] electric power utility wastes,[4−6] acidic mine wastes or tailings,[7] and agricultural runoff. Despite an extensive amount of work on the environmental chemistry of many of these species,[8−10] predictive capability for the migration of many of these species in the subsurface is still extremely limited. This is due, in part, to lack of adequate characterization of the structural aspects of the adsorption chemistry at key sites on oxide surfaces that can dominate the overall uptake of these species.

Recently, molecular modeling methods, based on empirical force fields, have been developed that can simulate the surface protonation, relaxation, and charging of ferric oxide surfaces, one of the most environmentally important adsorbing surfaces for oxyanions.[11−16] These models have demonstrated the importance of differences in site heterogeneity and bonding on the uptake of protons and on the development of localized surface charge and bond energies. It is anticipated that such differences in site binding will have a dramatic effect on the uptake of oxyanions at different sites on the oxide surface. The basis for the method is a linear free energy relationship between gas-phase cluster protonation energies and solution pK_a's for hydrolysis reactions. This relationship is applied to protonation reactions on mineral surfaces to generate surface pK_a's (which are not known experimentally) to predict the surface charge development on iron oxide surfaces.

It is therefore of interest to evaluate whether such an approach can be extended to the binding of environmentally important oxyanions in order to better understand the site-specific binding of these species to important oxide and mineral surfaces. Experimental equilibrium constants for aqueous hydrolysis reactions have been used for many years to understand and quantify the acid−base chemistry of oxide surfaces.[17−20] However, the connection between aqueous solution and the oxide−water interface is most often made by using gas-phase arguments based on Pauling bond strengths or electronegativities.[21] An implicit assumption is that differential solvation effects and differential entropies are of minor importance. The lack of a procedure for explicitly extricating solvent effects may inhibit attempts to understand surface chemistry by analogy with aqueous chemistry, as solvation effects may have quite different manifestations on surfaces. The gas-phase proton binding energies, if available, provide a less biased set of data on which to build the surface-aqueous analogy.

The major goal of this work is to determine whether gas-phase acidities for selected oxyanions can be correlated with known pK_a's in solution. The gas-phase acidities have been calculated by the ab initio electronic structure approach, density functional theory (DFT). This is a necessary first step in determining the effects of solvation or protonation on the oxyanions and hence the degree to which they will exhibit site selectivity at different sites on the oxide surface.

II. Methods

Continuing our previous work on trivalent ion hydrolysis reactions,[22] we have calculated the energies and vibrational frequencies of six tetrahedral oxyanions, in all of their relevant protonation states, using DFT.[23,24] DFT has been shown to be a reliable approach for the calculation of molecular geometries, vibrational frequencies, and energetics for a broad range of main group and transition metal-derived molecules.[25−32] The molecules studied here are H_2CrO_4, H_2SO_4, H_3PO_4, H_3VO_4, H_3AsO_4, and H_4SiO_4. These molecules represent three formal oxidation states (+6, +5, and +4), with first acid dissociation pK_a's ranging from −3 (H_2SO_4) to 10 (H_4SiO_4).

The calculations were done with the DFT program DGauss[33] and the program system Gaussian 94.[34] Two sets of calculations were done. The Gaussian 94 optimizations and frequency calculations were done with the hybrid B3LYP exchange-correlation functional, a generalized gradient functional. For these calculations, the 6-311++G** basis was used for O and H and the McLean and the Chandler negative ion basis set for

† Pacific Northwest National Laboratory.
‡ Pennsylvania State University.

10.1021/jp993421f CCC: $19.00
Published on Web 04/01/2000

TABLE 1: T−O Bond Lengths and Symmetric Stretch Frequencies for Unprotonated Species[a]

		T−O (pm)	ν_s TO_4 (a_1)	δ TO_4 (e)	ν_{as} TO_4(t_2)	δ TO_4 (t_2)
SO_4^{2-}	B3LYP	152.6	865 (983)	399 (450)	995 (1105)	561 (611)
	LDFT	153.0	878	390	1044	551
CrO_4^{2-}	B3LYP	165.7	859 (846)	336 (349)	871 (890)	382 (378)
	LDFT	166.5	853	323	903	365
PO_4^{3-}	B3LYP	160.6	789 (938)	349 (420)	845 (1017)	494 (567)
	LDFT	160.4	796	348	918	501
VO_4^{3-}	B3LYP	174.0[b]	777 (826)			
	LDFT	174.4[c]	760	294	335	786
AsO_4^{3-}	B3LYP	175.5	661 (837)	272 (349)	648 (878)	350 (463)
	LDFT	175.0	681	275	708	364

[a] Experimental numbers in parentheses are taken from ref 48. [b] VO_4^{3-} is not predicted to have T_d symmetry at the B3LYP level, so only the breathing mode is compared. [c] VO_4^{3-} is predicted to have approximate T_d symmetry at the LDFT level.

S, P, and Si.[35,36] For V and Cr, the Wachters−Hay[37,38] all electron basis set was used with scaling factors from Raghavachari and Trucks.[39] For As, the basis set was taken from Curtiss and co-workers.[40] The DGauss optimizations and frequency calculations were done at the local level with the potential fit of Vosko, Wilk, and Nusair[42] The DZVP2 basis set[41] (and A1 fitting set) was used on all molecules except for the As compounds. For the As compounds, the calculations were done with the DZVP basis set on As and the DZVP2 basis on O and H. At the final local geometries, gradient-corrected energies (BP) were obtained with the nonlocal exchange potential of Becke[43] combined with the nonlocal correlation functional of Perdew.[44]

As there are no reliable experimental values for the gas-phase acidities for these acids, we have used the G2[45] and CBS-4[46] methods to calculate the acidities of the second row species H_4SiO_4, H_3PO_4, and H_2SO_4 for calibration purposes. The G2 and CBS-4 calculations were started from the LDFT geometries and these calculations were done with Gaussian94.

III. Results

A. Structure. For these compounds, there are five types of structures for $[TO_4H_n]^m$ for $n = 0-4$ and $m = 0$ to -4. The results are summarized in Tables 1−5.The five structural types are shown in Figure 1 with T = P. The structures do show some variation depending on T. For example, for $n = 1$, the OH bond may be staggered with respect to two T−O bonds or it may eclipse a T−O bond. For $n = 4$, there can be significant deviation from tetrahedral bond angles, although the orientations of the protons remain similar. As shown in Tables 1−5, all molecules showed considerable similarity on progression from $[TO_4]^{m=-2to-4}$ to $[HTO_4]^{m=-1to-3}$ to $[H_2TO_4]^{m=0to-2}$ to $[H_3TO_4]^{m=+1to-1}$ to $[H_4TO_4]^{m=+2to0}$, where the charges depend on the oxidation state of T, and the variations did not show a strong dependence on the specific molecular charge. The first step, going from TO_4 to HTO_4, is accompanied by a substantial lengthening of the T−OH bond (10−15%) and a small shortening of the T−O bonds. The T(VI) ions, HSO_4^- and $HCrO_4^-$, have an OH bond staggered with respect to TO, while the $T^{V}H(As,V,P)O_4^{2-}$ and $T^{IV}HSiO_4^{3-}$ ions have eclipsed arrangements. The H_2TO_4 structures are similar, with a 4−6% increase in the T−OH bonds and a 4−6% decrease in the T−O bonds with respect to the $(TO_4)^{m-}$ ion. For the H_3TO_4 strucures, there is a 6−7% decrease in the T−O bond and a very small increase in the T−OH bond. Finally, H_4TO_4 structures have T−OH bonds about 2% shorter than the T−O bonds in the $(TO_4)^{m-}$ anions.

TABLE 2: T−OH and T−O Bond Lengths and Key Vibrational Frequencies for Singly Protonated Species[a]

		T−OH	T−O	δ TOH	ν_{as} TO_3	ν_s TO_3	ν_s T−OH	ν OH
HSO_4^-	B3LYP	171.9	147.3*,[g] 148.6	1241[b]	1181, 1241[c]	988	670	3810
	LDFT	170.1	148.7*, 147.7	1096[b]	1207, 1263[c]	1002	702	3693
$HCrO_4^-$	B3LYP	184.2	160.3*, 160.6	785	1019, 1001	968	637	3841
	LDFT	180.4	161.8*, 161.1	778	1034, 1015	956	677	3727
HPO_4^{2-}	B3LYP	178.3	156.1, 154.5*	1099[c] (1240)	1083 (1080)	898 (980)	587[e] (870)	3834
				974	1114	902	462[f]	3636
	LDFT	176.5	156.4, 154.4*	1140[d]			626[e]	
				986			473[f]	
HVO_4^{2-}	B3LYP	197.7	168.7, 168.1*	880[b]	871	862	499	3854
	LDFT	193.4	169.4, 168.5*		920	868	537	3702
				929[b]				
				730				
$HAsO_4^{2-}$	B3LYP	193.5	170.9, 169.4*	1004	808, 790	750	442	3798
	LDFT	191.4	171.0, 169.0*	1107	846, 822	766	475	3522

[a] Distances are in picometers, and frequencies are in cm^{-1}. Experimental values for hydrogen phosphate in parentheses are taken from ref 49. The following footnotes show mixing of modes. [b] + TO_3 asym. [c] + δ_{TOH}. [d] + ν_{as} PO_3. [e] + inv. [f] -inv. [g] Asterisk refers to x2.

TABLE 3: T−OH and T−O Bond Lengths and Key Vibrational Frequencies for Doubly Protonated Species[a]

		T−OH	T−O	ν_{as} TO_2	ν_s TO_2	ν_{as} $T(OH)_2$	ν_s $T(OH)_2$	ν OH
H_2SO_4	B3LYP	162.6	143.9	1413 (1450)	1166 (1223)	810 (883)	758 (834)	3761, 3757
	LDFT	162.2	145.0	1418	1169	831	771	
H_2CrO_4	B3LYP	175.8	156.0	1108	1084	786, 734[b]	763[b]	3812, 3807
	LDFT	174.1	157.6	1101	1053	813, 758[b]	768[b]	
$H_2PO_4^-$	B3LYP[c]	168.1	150.7	1293 (1150)	1064 (1070)	751 (943)	729 877)	3843, 3842
	LDFT[d]	167.0	151.0	1295	1069	792	747	3715, 3715
$H_2AsO_4^-$	B3LYP	183.2	165.4	917	849	579	586	3817, 3816
	LDFT	181.8	165.5	930	863	611	604	
$H_2VO_4^-$	B3LYP	186.3	162.3	1004	995	637	628	3867, 3866
	LDFT	183.6	163.5	1017	979	671	639	
$H_2SiO_4^{2-}$	B3LYP	178.6	160.7	1085[b]	876	630	608	3831, 3831
	LDFT	177.1	161.0	946[b]	880	667	625	

[a] Distances are in picometers, and frequencies are in cm^{-1}. Experimental values in parentheses are taken from ref 50 for sulfuric acid and from ref 49 for the dihydrogen phosphate ion. [b] Strongly coupled to δTOH mode. [c] POH asym bend at 1045 and POH sym bend at 1030. [d] POH asym bend at 1031 and POH sym bend at 1011.

TABLE 4: T−OH and T−O Bond Lengths and Key Vibrational Frequencies for Triply Protonated Species[a]

		T−O	T−OH	ν TO	ν_s T(OH)$_3$	ν OH
H_3PO_4	B3LYP	147.7	161.6, 161.2	1322 (1258)	804 (891)	3837, 3828, 3823
	LDFT	148.4	160.4 × 3	1290	824	3726, 3722, 3722
H_3AsO_4	B3LYP	162.1	176.6 × 2, 176.0	963	668	3811, 3797, 3795
	LDFT	162.9	175 × 3	968	695	3644, 3642, 3642
H_3VO_4	B3LYP	156.6	178.5, 177.6 × 2	1115	717	3862, 3857, 3821
	LDFT	158.6	176.3 × 3	1078	742	3750, 3741, 3741
$H_3SiO_4^-$	B3LYP	156.3	171.1 × 2, 169.8	1114	699	3892, 3887, 3878
	LDFT	156.4	170.3 × 2, 169.1	1120	708	3779, 3776, 3776

[a] Distances are in picometers, and frequencies are in cm^{-1}. Experimental values for orthophosphoric acid in parentheses are taken from ref 52.

TABLE 5: T−OH and T−O Bond Lengths and Key Vibrational Frequencies for Quadruply Protonated Species[a]

		T−OH	T−OH sym str	OH str (symm)
$H_4PO_4^+$	B3LYP	156.5	831−934[b]	3783
	LDFT	155.9	844−899[b]	3657
$H_4AsO_4^+$	B3LYP	171.3	707	3743
	LDFT	170.9	727	3568
$H_4VO_4^+$	B3LYP	168.8	794	3776
	LDFT	170.5	802	3663
H_4SiO_4	B3LYP	164.6	757	3901
	LDFT	164.1	762	3789

[a] Distances are in picometers, and frequencies are in cm^{-1}. [b] Very mixed with δTOH.

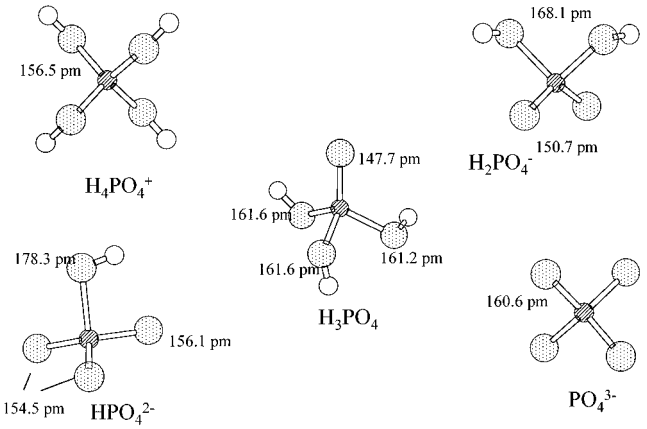

Figure 1. Changes in oxyacid structure as a function of protonation state. The example shown in the figure is for $H_nPO_4^{n-3}$. $H_4PO_4^+$ is included for completeness in establishing trends; the species is not known to exist in aqueous solution.

For sulfuric acid, structure predictions can be compared to microwave spectroscopy measurements.[47] A detailed comparison is shown in Table 6. Theory predicts S−O distances that are somewhat too long; otherwise the agreement between theory and experiment is quite good.

B. Vibrational Spectra. Selected vibrational frequencies are also reported in Tables 1−5. The vibrational frequencies provide useful insight into the response of the molecular structure to protonation/deprotonation reactions as well as providing a useful test of the DFT calculations. A number of experimental determinations of vibrational spectra exist for comparison with the calculated values. For the unprotonated TO_4 ions, the comparison is given in Table 1. The B3LYP DFT stretching frequencies are lower than the LDFT values, as expected from many previous studies. In general, for these ions, there is a clear tendency for the DFT methods to underestimate the vibrational frequencies, although the differences by which the frequencies differ vary from ion to ion. The differences between theory and experiment are substantially larger than usually found and this

TABLE 6: Comparison of the Calculated H_2SO_4 Structure with Experiment[a]

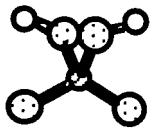

	DFT B3LYP	LDFT	ref 47
r(OH)	97.0	98.6	97.0 ± 1
r(SO_1)	162.6	162.2	157.4 ± 1
r(SO_2)	143.9	145.2	142.2 ± 1
∠HOS	109.5	107.6	108.5 ± 1.5
∠$O_1SO_{1'}$	101.5	101.7	101.3 ± 1
∠$O_2SO_{2'}$	124.6	125.4	123.3 ± 1
∠O_1SO_2	108.9	108.4	108.6 ± 0.5
∠$O_1SO_{2'}$	105.3	105.3	106.4 ± 0.5
∠$H_1O_1SO_2$	30.5	26.1	20.8 ± 1
∠$H_1O_1SO_{1'}$	−80.3	−84.6	−90.9 ± 1

[a] Distances are in picometers, and angles are in degrees. O_1 and O_1' are the oxygens bonded to H_1 and H_1', respectively, and O_2 and O_2' are the "doubly bonded" oxygens.

is at least partly due to the fact that the vibrational frequencies of the unprotonated anions are measured in the solid phase[48] where there can be significant interactions with the cations in the matrix.

For the HTO_4 ions, only the infrared and Raman spectra of aqueous HPO_4^{2-} have been measured experimentally.[49] As shown in Table 2, the agreement is generally good, although we do question some of the assignments. We note that the 980 cm^{-1} peak assigned to the symmetric TO_3 stretching mode is close to the calculated 974 (B3LYP) and 986 (LDFT) cm^{-1} mode assigned to δPOH in our DFT calculations. This mode is strongly coupled with a PO_3 mode in which the eclipsed PO bond stretch vibrates asymmetrically with the two other PO bond stretches. This asymmetric PO stretching mode is calculated to be at 1099 (B3LYP) and 1140 (LDFT) cm^{-1}. We also note that the P−OH stretching mode is strongly coupled to the PO_3 inversion bend.

For the H_2TO_4 species, the most extensive measurements (vapor phase) exist for sulfuric acid.[50] A detailed comparison of the band assignments is shown in Table 7. The agreement between theory and experiment is good and supports the previous assignments,[50] except that we note significant mixing between the asymmetric SO_2 stretch and the asymmetric coupling of the SOH bends. The calculated values are generally less than the experimental ones, consistent with the fact that the calculated bond distances are longer than the experimental ones.

The infrared spectrum of aqueous $H_2PO_4^-$ has been reported.[49] The calculated value for the asymmetric TO_2 stretch (1293 cm^{-1}) is considerably higher than the observed band at 1150 cm^{-1}, which is somewhat surprising considering the H_2-

TABLE 7: Comparison between Theory and Experiment for the Vibrational Frequencies and Band Assignments for Sulfuric Acid

		DFT	ref 50
OH str	B3LYP	3760 (s), 3756 (as)	3610
	LDFT	3649 (s), 3645 (as)	
SO_2 asym str	B3LYP	1413 + asym OH bend	1450
	LDFT	1418 + asym OH bend	
SO_2 sym str	B3LYP	1165 + sym OH bend	1223
	LDFT	1169 + sym OH bend	
SOH asym bend	B3LYP	1137	1159, 1138[a]
	LDFT	1120 + SO_2 asym str	
SOH sym bend	B3LYP	1127	1159, 1138[a]
	LDFT	1090	
$S(OH)_2$ asym str	B3LYP	810	883
	LDFT	831	
$S(OH)_2$ sym str	B3LYP	758	834
	LDFT	771	
SO_2 rock	B3LYP	517	568
	LDFT	501	
SO_2 bend	B3LYP	510	550
	LDFT	489	
$S(OH)_2$ rock	B3LYP	470	
	LDFT	447	
$S(OH)_2$ sym torsion	B3LYP	422	
	LDFT	418	
$S(OH)_2$ bend	B3LYP	360	
	LDFT	336	
$S(OH)_2$ asym torsion	B3LYP	314	
	LDFT	330	
SO_4 twist	B3LYP	260	
	LDFT	252	

[a] These frequencies were not assigned to symmetric and asymmetric components in the original paper.[50]

SO_4 results. This is possibly due to hydrogen bonding perturbations in the aqueous measurements, which should decrease the frequency from that of the free ion. Calculations of the symmetric stretch for $H_2PO_4^-$ at 1064 cm^{-1} (B3LYP) and 1069 cm^{-1} (LDFT) are consistent with the assignment for the peak observed at 1070 cm^{-1},[49,51] although it is interesting that the hydrogen bonding interactions, if present, do not appear to affect $\nu_s(PO_2)$ as much as $\nu_{as}(PO_2)$. Both the asymmetric and symmetric combinations of the P−(OH) stretching modes appear to be underestimated by the DFT calculations, although we note that the POH bends at 1000−1050 cm^{-1} have enough intensity to have been easily observed in the infrared and are closer to the 943 and 877 cm^{-1} values reported for the P−OH stretching.

The Raman spectrum of aqueous orthophosphoric acid has been reported.[52] A band at 1173 cm^{-1} at 25° C was assigned to the P−O stretching mode. As the temperature increased to 450° C, the frequency of this band increased to 1258 cm^{-1}. The authors hypothesized that this increase in frequency is due to the decreasing perturbation of hydrogen bonding on the P−O stretch as temperature increases. The calculated values of 1322 cm^{-1} (B3LYP) and 1290 cm^{-1} (LDFT) are in reasonable agreement with the high-temperature value, supporting this interpretation. A band at 891 cm^{-1} at 25 °C was assigned to the symmetric combination of the P−(OH) stretch. Our calculations suggest that the symmetric stretch is nearly 100 cm^{-1} lower, at 804 cm^{-1} (B3LYP) and 824 cm^{-1} (LDFT). There are asymmetric combinations of the P−(OH) stretching modes at 884 and 899 cm^{-1} (B3LYP) and 920 and 918 cm^{-1} (LDFT). The asymmetric combinations of the POH bends (1029 and 1019 cm^{-1} (B3LYP); 1033 and 1028 cm^{-1} (LDFT)) are strongly coupled to the asymmetric combinations of the P−OH stretches. The symmetric combination of the POH bends is at 985 cm^{-1} (B3LYP) and 1016 cm^{-1} (LDFT).

TABLE 8: Energy Differences for Calculating PAs

		neutrals		monoanions		dianions	
		$-\Delta E_{elec}$	ΔZPE	$-\Delta E_{elec}$	ΔZPE	$-\Delta E_{elec}$	ΔZPE
Cr	B3LYP	321.0	−7.1	455.8	−6.8		
	BP	321.1	−6.8	456.3	−6.6		
S	B3LYP	315.2	−7.6	452.3	−7.3		
	BP	316.7	−7.4	457.0	−6.9		
P	B3LYP	330.9	−7.2	461.7	−7.9	583.8	−7.4
	BP	331.7	−7.2	465.9	−7.3	599.1	−7.2
V	B3LYP	331.4	−6.9	461.8	−7.3	563.5	−7.6
	BP	333.2	−6.5	463.4	−6.9	589.9	−6.7
As	B3LYP	329.7	−7.1	456.3	−7.4	574.0	−7.4
	BP	332.8	−6.8	462.7	−7.1	592.0	−7.1
Si	B3LYP	357.2	−7.4	472.4	−7.2		
	BP	356.6	−7.3	477.2	−7.2		

We note that, for a given T−O bond length, there appears to be a tendency for the transition metal oxyacids to have much lower T−O−H bending frequencies than the main group oxyacids. This is especially true for the H_2TO_4 species; for example, the δTOH modes for $H_2AsO_4^-$ (d_{TO} = 183.2 pm (B3LYP) and 181.8 pm (LDFT)) are predicted to be 1046 cm^{-1} (B3LYP) and 1059 cm^{-1} (LDFT) and 1011 cm^{-1} (B3LYP) and 1022 cm^{-1} (LDFT), whereas those for $H_2VO_4^-$ (d_{TO} = 186.3 pm (B3LYP) and 183.6 pm (LDFT)) are 696 cm^{-1} (B3LYP) and 716 cm^{-1} (LDFT) and 692 cm^{-1} (B3LYP) and 699 cm^{-1} (LDFT). This may have some significance for surface complexation reactions as the transition metal oxyacids may be able to have more flexible hydrogen bonds to the surface.

C. Gas-Phase Proton Affinities. The proton affinity of a monovalent anion (related to the acidity) can be defined as the negative of the enthalpy change for the following reaction calculated at 0 K:

$$H^+ + A^- \rightarrow HA \quad (1)$$

The enthalpy change at 0 K consists of the electronic energy difference between HA and A^- together with a correction for the difference in zero point energies.

$$PA(A^-) = -[(E_{elec}\{HA\} - E_{elec}\{A^-\}) + (ZPE\{HA\} - ZPE\{A^-\})] \quad (2)$$

Defined in this way, the proton affinity of A^- is a positive number; the more positive the number, the greater is the energy gained by the system upon association of H^+ with A^-. To convert the 0 K value to 298 K, one has to include thermal corrections for the translational, rotational, and vibrational energies and a correction for the change in the number of molecules assuming ideal gas behavior. Assuming no temperature dependence on the vibrational energies, one gets a correction of 2.5*RT*. We can extend the definition of $PA(A^-)$ to include anions with negative charge *n*:

$$H^+ + A^{-n} \rightarrow HA^{-n+1} \quad (3)$$

giving

$$PA(A^{-n}) = -[(E_{elec}\{HA^{-n+1}\} - E_{elec}\{A^{-n}\}) + (ZPE\{HA^{-n+1}\} - ZPE\{A^{-n}\})] \quad (4)$$

The values for $-\Delta E_{elec}$, ΔZPE, and $PA(A^n)$ are given in Tables 8 and 9.

The B3LYP and BP values for the PAs of A^- are in good agreement with each other with the largest difference found for

TABLE 9: Charges (e), Radii (pm), Gas-Phase Acidities (GPA) (kcal/mol), pK_a for Tetrahedral Oxyacids[a]G

				neutrals		monoanions		dianions	
	Z	radius	Z/r	PA	pK_a^1	PA	pK_a^2	PA	pK_a^3
Cr	6	40	0.1500	313.9	−0.2	449.0	6.15		
BP				314.3		449.7			
S	6	26	0.2308	307.6	−1.98	445.0	1.99		
BP				309.3		450.1			
P	5	31	0.1613	323.7	2.15	453.8	7.20	576.4	12.35
BP				324.5		458.6		591.9	
V	5	49.5	0.1010	324.5	4.00	454.5	8.55	555.9	14.3
BP				326.7		456.5		583.2	
As	5	47.5	0.1053	322.6	2.24	448.9	6.96	566.6	11.5
BP				326.0		455.6		584.9	
Si	4	40	0.1000	349.8	9.86	465.2	13.1		
BP				349.3		470.0			

[a] GPAs were calculated using DFT as described in the text. pK_a's are taken from ref 55 except for pK_a^1 for H_2SO_4, which is taken from ref 18. Radii are taken from ref 56.

TABLE 10: G2 and CBS-4 PA(A^-) (Including Zero-Point Corrections) for T = Si, P, and S in kcal/mol

method	Si	P	S
G2 (0 K)	351.7	327.4	310.8
G2 (298 K)	353.1	328.4	312.2
CBS-4 (0 K)	350.1	324.0	307.7
CBS-4 (298 K)	351.4	324.9	308.4

T = As with a difference of ∼4 kcal/mol. The B3LYP and BP PAs of A^{2-} show larger differences with the largest being 7 kcal/mol (1.5%) for T = As again. The larger BP values are consistent with the lack of additional diffuse functions in the basis sets used at the BP level so that the more negatively charged species are less stabilized. The PAs for A^{3-} show even larger differences, and again the BP values are more negative, consistent with the basis set argument.

The values of PA(A^-) for $H_3SiO_4^-$, $H_2PO_4^-$, and HSO_4^- have been calculated at the G2 and CBS-4 levels (Table 10). We take the G2 values to be the most accurate set of calculations. The G2 values are consistently larger than the CBS-4 values in terms of the magnitude ranging from 1.6 kcal/mol for T = Si to 3.4 kcal/mol for T = P. Comparing the BP values to the G2 values, we note that the BP values are always of smaller absolute magnitude. The BP acidities of H_4SiO_4, H_3PO_4, and H_2SO_4 are 2.4, 2.9, and 1.5 kcal/mol less than the G2 values, in excellent agreement considering the level (and computational cost) of the BP calculations.

D. Relation between Gas-Phase Proton Affinity and Solution pK_a. Size/charge ratios have been previously used to rationalize the relative acidities of oxyanions.[18] The acidity of an oxyanion is usually defined in terms of pK_a, where K_a is the equilibrium constant for the reaction $HA^{-n+1}(aq) \rightarrow H^+(aq) + A^{n-}(aq)$:

$$K_a = [H^+][A^{n-}]/[HA^{-n+1}] \quad (5)$$

In Figure 2a,b, the size/charge correlation is shown for the oxyacids considered here. Clearly, it would be desirable to improve on the size/charge correlation. In this section, we investigate how the calculated gas-phase acidities correlate with the aqueous acidities of these oxyacids.

As shown in Figure 3a,b, the correlation between PA(A^n) and pK_a is good for the proton affinities of both the neutrals and monoanions. No such good correlation appears to exist for the dianions, which likely indicates the greater influence of solvation effects in determining the acidity constants of the dianions, as well as the difficulty in reliably calculating multiply charged anionic species. The neutrals and monoanions lie on two distinct lines, as shown in Figure 4, separated in energy by about 100 kcal/mol.

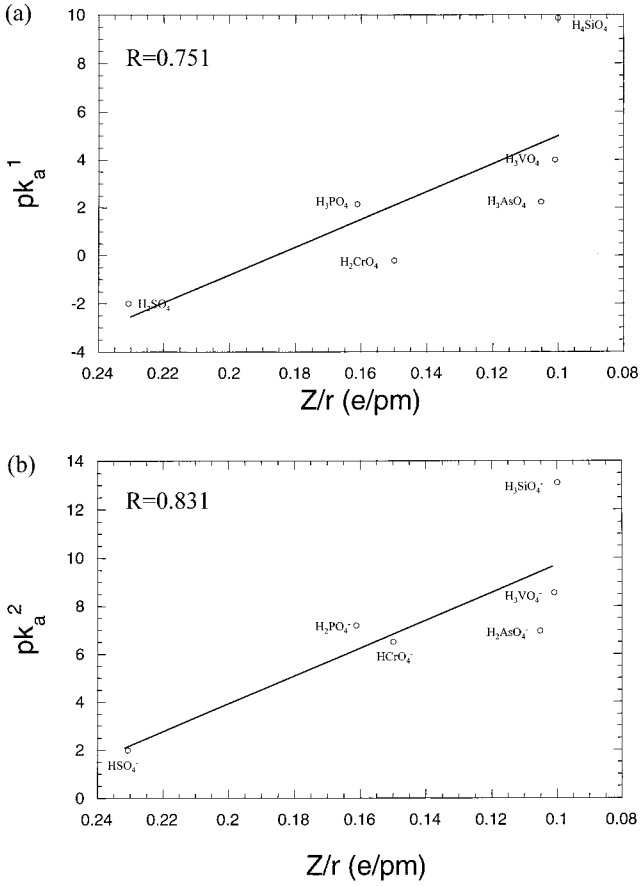

Figure 2. pK_a versus charge/size ratio for the oxyacids considered in this paper: (a) neutral molecules; (b) monoanions.

The present acidity calculations can be placed in context with other calculations (at the DFT level) on the gas-phase acidities of trivalent (+3) hexaaquo ions,[22] and the higher hydrolysis reactions for ferric iron in solution, calculated by successive deprotonation of $Fe(H_2O)_6^{3+}$, as shown in Figure 4. The pK_a vs ΔPA(A^n) slope for the deprotonation constants for the silicate and sulfate species are fairly consistent with the slope $\Delta pK_a/\Delta PA(A^n) = -0.028$ previously developed to estimate the surface charging behavior of goethite,[11,13] hematite,[15] and silica.[16] This relationship was determined from molecular mechanics calculations of deprotonation energies. The quantum-mechanically derived $\Delta pK_a/\Delta PA(A^n)$ slope is much the same as that derived from molecular mechanics for the species considered previously ($Fe(OH)_n$, $H_nSiO_4^{(n-4)}$). The $H_n(V,As,P)O_4^{(n-3)}$ species still appear to follow a linear trend, but the slope is steeper, close to the 0.04 pK_a/(kcal/mol) slope shown by the solid line. Thus, although there is a rough consistency with the 0.028 pK_a/(kcal/mol), the slope cannot be regarded as universal. The relative values of H_2SO_4 and HSO_4^- are closer to the 0.028 pK_a/(kcal/mol), but this must be regarded with caution, as the experimental value for H_2SO_4 is likely to be highly uncertain. The closeness of the intercepts for the silicate acidities and the iron hydrolysis constants is accidental. The wide scatter in the intercept values apparent in Figure 4 implies that, if one were to consider mixed systems such as Fe−PO_4 complexes or surface species, a different approach would be required. The intercepts, and ultimately the pK_a values, are specific to a given anion. Thus,

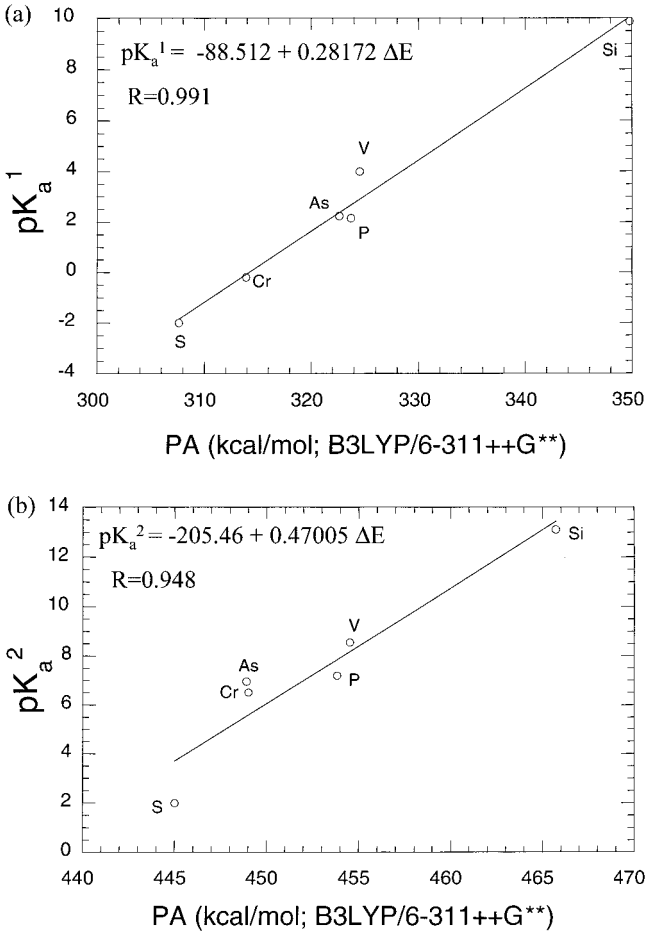

Figure 3. pK_a versus gas-phase acidity: (a) neutral molecules; (b) monoanions.

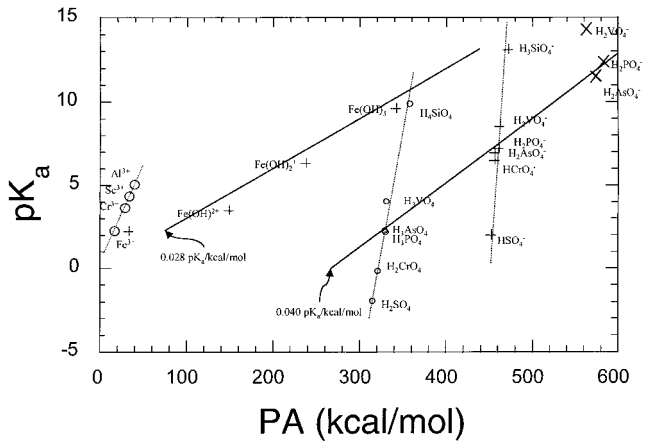

Figure 4. Global relationship between gas-phase acidity and pK_a for tripositive cations, ferric hydrolysis species, and neutral, monoanionic, and dianionic oxyanions. The two values for the deprotonation of Fe$(H_2O)_6^{3+}$ result from using two different basis sets: the DZVP (denoted by ○) and 6-311G (denoted by +). The solid line has a slope of 0.04 pK_a/(kcal/mol), and the dash−dot line has a slope of 0.028 pK_a/(kcal/mol).

there is no basis for prediction of the acidity of, for example, an Fe−O−POH_3 functional group because its associated intercept cannot be determined a priori. Extending the model to account for such species will require explicit solvation effects to be built into the model.

Another aspect of Figure 4 is the progressive increase in the pK_a/ΔPA(A^{n-}) slopes from the tripositive cations to monoanions

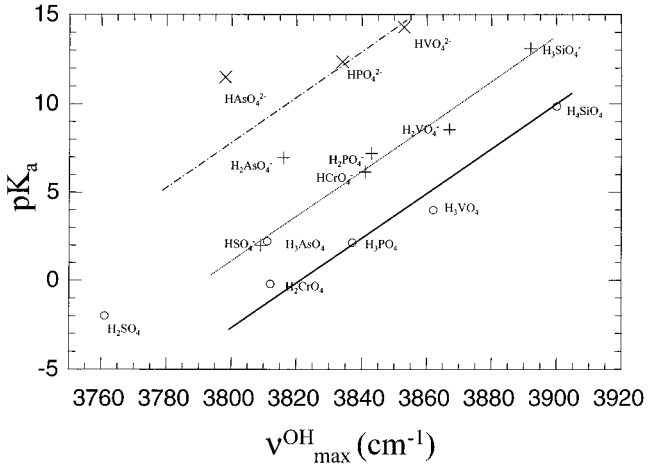

Figure 5. pK_a versus ν^{OH}_{max}, the highest OH stretching frequency for neutrals (○), monoanions (+), and dianions (×).

(the pK_a/ΔPA(A^{n-}) slope defined by the dashed lines in Figure 4). For two species on a given line

$$pK^1 = 1/RT\{\Delta G_g^{\,1} + \Delta G_s^{\,1}\} \quad \text{(I)}$$

$$pK^2 = 1/RT\{\Delta G_g^{\,2} + \Delta G_s^{\,2}\} \quad \text{(II)}$$

where $\Delta G_g = G^A - G^{HA}$ is the gas-phase deprotonation energy and $\Delta G_s = G_s^A - G_s^{HA}$ is the difference in solvation free energy between the product A and reactant HA. Ignoring changes in entropy, and equating ΔG_g with ΔE_g, the gas-phase deprotonation energy calculated as described above (i.e., $pK^1 = 1/RT\{\Delta E_g^{\,1} + \Delta G_s^{\,1}\}$), the slope of the line is

$$pK_2 - pK_1/(PA(2) - PA(1)) = 1/2.303RT\{1 + (\Delta G_s^{\,2} - \Delta G_s^{\,1})/(PA(2) - PA(1))\} \quad \text{(III)}$$

If there were no effect from solvation, the slope should be approximately 0.73 pK_a/(kcal/mol) (1/2.303RT). For a given increase in proton binding energy, the solution phase acidity is *greater* than would be predicted by the 0.73 (1/2.303RT) slope. This implies that the reaction products are stabilized by the solvation free energy; $\Delta G_s^{\,2} - \Delta G_s^{\,1}$ is negative if PA(2) − PA(1) is positive. In other words, if a given compound A^{n-} has a high proton affinity, it is also has a high (favorable) solvation energy. Further elucidation of this relationship will be the subject of future work.

Previously, pK_a has been correlated with ν^{OH} the OH stretching frequency.[53,54] Figure 5 shows this correlation for the oxyanions and is very satisfactory, except for the apparently anomalous behavior of the $H_nAsO_4^{(n-3)}$ species. The dash−dot, dashed, and solid lines have the same slope and are derived from the best overall slope representing neturals, monoanions, and dianions not including $H_nAsO_4^{(n-3)}$ species. This type of correlation is extremely poor for the tripositive cations.[57]

IV. Summary

All of the oxyacids exhibit similar structural changes in terms of T−O bond lengthening/shortening upon protonation/deprotonation. The DFT calculations compare well with available experimental structural data. For fully deprotonated TO_4^{n-} ions, the DFT calculations show a clear tendency to underestimate vibrational frequencies. This tendency does not appear to be uniform among the oxyacids investigated here. For example, the vibrational frequencies of CrO_4^{2-} were within 2% of

experiment, but those for AsO_4^{3-} were 20% too low. This disagreement could be due to calculating the properties of isolated small anions with high negative charge, which are inherently unstable as free species. For protonated oxyacids, better agreement with the experimental frequencies is found. There exists a well-defined correlation between measured pK_a in aqueous solution and calculated gas-phase acidities. This relationship is significantly better than that obtained on the basis of charge/size criteria.

While the pK_a/ΔPA(A^n) slope used in previous studies of the surface charging of oxides[11,13,15,16] is fairly consistent from system to system, it is not universal. Furthermore, intercepts in the pK_a/ΔPA(A^n) correlations vary widely from anion to anion, posing additional challenges for the prediction of pK_a's in mixed systems, either in solution or for adsorbed complexes on surfaces.

Acknowledgment. This work was supported by the DOE EMSP program and the Office of Basic Energy Sciences, Engineering and Geosciences Division, contract 18328. Pacific Northwest Laboratory is operated for the U.S. Department of Energy by Battelle Memorial Institute under Contract DE-AC06-76RL0 1830. We are grateful to the National Energy Research Supercomputing Center for a generous grant of computer time.

References and Notes

(1) Stumm, W. *Chemistry of the Solid-Water Interface*; John Wiley and Sons: New York.

(2) Drever, J. I. *The Geochemistry of Natural Waters*, 2nd ed.; Prentice Hall: Englewood Cliffs, NJ, 1988.

(3) Riley, R. G.; Zachara, J. M. *Chemical Contaminations on DOE Lands and Selection of Contaminant Mixtures for Subsurface Science Research*; U.S. Department of Energy: Washington, DC, 1992.

(4) Rai, D.; Eary, L. E.; Zachara, J. M. *Sci. Total Environ.* **1989**, *86*, 15.

(5) Mattigod, S. V.; Rai, D.; Eary, L. E.; Ainsworth, C. C. *J. Environ. Qual.* **1990**, *19*, 188.

(6) Eary, L. E.; Rai, D.; Mattigod, S. V.; Ainsworth, C. C. *J. Environ. Qual.* **1990**, *19*, 202.

(7) Felmy, A. R.; Peterson, S. R.; Serne, R. J. *Uranium* **1987**, *4*, 25.

(8) Rai, D. *Attenuation Rates, Coefficients, and Constants in Leachate Migration: A Critical Review*; Electric Power Research Institute: 1984.

(9) Rai, D. *Geochemical Behavior of Chromium Species*: Electric Power Research Institute: 1986.

(10) Rai, D. *Chromium Reactions in Geologic Materials*; Electric Power Research Institute: 1988.

(11) Felmy, A.; Rustad, J. *Geochim. Cosmochim. Acta* **1998**, *62*, 25.

(12) Rustad, J. R.; Hay, B. P.; Halley, J. W. *J. Chem. Phys.* **1995**, *102*, 427.

(13) Rustad, J. R.; Felmy, A. R.; Hay, B. P. *Geochim. Cosmochim. Acta* **1996**, *60*, 1563.

(14) Rustad, J. R.; Felmy, A. R.; Hay, B. P. *Geochim. Cosmochim. Acta* **1996**, *60*, 1553.

(15) Rustad, J. R.; Wasserman, E.; Felmy, A. R. *Surf. Sci.* **1999**, *424*, 28.

(16) Rustad, J. R.; Wasserman, E.; Felmy, A. R.; Wilke, C. *J. Colloid Interface Sci.* **1998**, *198*, 119.

(17) Parks, G. A. *Chem. Rev.* **1965**, *65*, 177.

(18) Hiemstra, T.; Van Riemsdijk, W. H.; Bolt, G. H. *J. Colloid Interface Sci.* **1989**, *133*, 91.

(19) Sverjensky, D. A. *Geochim. Cosmochim. Acta* **1994**, *58*, 3123.

(20) Yoon, R. H.; Salman, T.; Donnay, G. *J. Colloid Interface Sci.* **1979**, *70*, 483.

(21) Nortier, P.; Borosy, A. P.; Allavena, M. *J. Phys. Chem.* **1997**, *101*, 1347.

(22) Rustad, J. R.; Dixon, D. A.; Felmy, A. R. *J. Am. Chem. Soc.* **1999**, *121*, 3234.

(23) Parr, R. G.; Yang, W. *Density Functional Theory of Atoms and Molecules*; Oxford University Press: New York, 1989.

(24) Labanowski, J.; Andzelm, J. *Density Functional Methods in Chemistry*; Springer-Verlag: New York, 1991.

(25) Sosa, C.; Andzelm, J.; Elkin, B. C.; Wimmer, E.; Dobbs, K. D.; Dixon, D. A. *J. Phys. Chem.* **1992**, *96*, 6630.

(26) Christe, K. O.; Dixon, D. A. *J. Am. Chem. Soc.* **1992**, *114*, 2978.

(27) Christe, K. O.; Dixon, D. A.; Goldberg, I. B.; Schack, C. J.; Wang, J. T.; Walther, B.; Williams, F. *J. Am. Chem. Soc.* **1993**, *115*, 1129.

(28) Christe, K. O.; Curtis, E. C.; Dixon, D. A. *J. Am. Chem. Soc.* **1993**, *115*, 1520.

(29) Christe, K. O.; Dixon, D. A.; Mahjoub, A. R.; Mercier, H. P.; Sanders, J. C. P.; Seppelt, K.; Schrobilgen, G. J.; Wilson, W. W. *J. Am. Chem. Soc* **1993**, *115*, 2696.

(30) Christe, K. O.; Dixon, D. A.; Sanders, J. C. P.; Schrobilgen, G. J.; Wilson, W. W. *J. Am. Chem. Soc.* **1993**, *115*, 9461.

(31) Christe, K. O.; Curtis, E. C.; Dixon, D. A. *J. Am. Chem. Soc.* **1993**, *115*, 9655.

(32) Christe, K. O.; Dixon, D. A.; Sanders, J. C. P.; Schrobilgen, G. J.; Wilson, W. W. *Inorg. Chem.* **1993**, *32*, 4089.

(33) DGauss DGauss is a density functional program which is part of Unichem and is available from Oxford Molecular.

(34) Frisch, M. J.; Trucks, G. W.; Schlegel, H. B.; Gill, P. M. W.; Johnson, B. G.; Robb, M. A.; Cheeseman, J. R.; Keith, T. A.; Petersson, G. A.; Montgomery, J. A.; Raghavachari, K.; Al-Laham, M. A.; Zakrzewski, V. G.; Ortiz, J. V.; Foresman, J. B.; Cioslowski, J.; Stefanov, B. B.; Nanayakkara, A.; Challacombe, M.; Peng, C. Y.; Ayala, P. Y.; Chen, W.; Wong, M. W.; Andres, J. L.; Replogle, E. S.; Gomperts, R.; Martin, R. L.; Fox, D. J.; Binkley, J. S.; Defrees, D. J.; J. Baker; Stewart, J. P.; Head-Gordon, M.; Gonzalez, C.; Pople, J. A. *Gaussian 94*; Gaussian, Inc.: Pittsburgh, PA, 1995.

(35) McLean, A. D.; Chandler, G. S. *J. Chem. Phys.* **1980**, *72*, 5639.

(36) Krishnan, R.; Binkley, J. S.; Seeger, R.; Pople, J. A. *J. Chem. Phys.* **1980**, *72*, 650.

(37) Wachters, A. J. H. *J. Chem. Phys.* **1970**, *52*, 1033.

(38) Hay, P. J. *J. Chem. Phys.* **1977**, *66*, 4377.

(39) Raghavachari, K.; Trucks, G. W. *J. Chem. Phys.* **1989**, *91*, 1062.

(40) Curtiss, L. A.; McGrath, M. P.; Blaudeau, J.-P.; Davis, N. E.; R. C. Binning, J.; Radom, L. *J. Chem. Phys.* **1995**, *103*, 6104.

(41) Godbout, N.; Salahub, D. R.; Andzelm, J.; Wimmer, E. *Can. J. Chem.* **1992**, *70*, 560.

(42) Vosko, S. J.; Wilk, L.; Nusiar, M. *Can. J. Phys.* **1980**, *58*, 1200.

(43) Becke, A. D. *Phys. Rev. A* **1988**, *38*, 3098.

(44) Perdew, J. P. *Phys. Rev. B* **1986**, *33*, 8822.

(45) Curtiss, L. A.; Raghavachari, K.; Trucks, G. W.; Pople, J. A. *J. Chem. Phys.* **1991**, *94*, 7221.

(46) Ochterski, J. W.; Petersson, G. A.; Montgomery, J. A. *J. Chem. Phys.* **1996**, *104*, 2598.

(47) Kuczkowski, R. L.; Suenram, R. D.; Lovas, F. J. *J. Am. Chem. Soc.* **1981**, *103*, 2561.

(48) Nakamoto, K. *Infrared and Raman spectra of inorganic and coordination compounds. Part A: Theory and applications in inorganic chemistry*; John Wiley and Sons: New York, 1997.

(49) Steger, V. E.; Herzog, K. *Z. Anorg. Allg. Chem.* **1964**, *331*, 169.

(50) Chackalackal, S. M.; Stafford, F. E. *J. Am. Chem. Soc.* **1966**, *88*, 723.

(51) Preston, C. M.; Adams, W. A. *J. Phys. Chem.* **1979**, *83*, 814.

(52) Marshall, W. L.; Begun, G. M. *J. Chem. Soc., Faraday Trans. 2* **1989**, *85*, 1963.

(53) Kubicki, J. D.; Xiao, Y.; Lasaga, A. C. *Geochim. Cosmochim. Acta* **1993**, *57*, 3847.

(54) Kubicki, J. D.; Blake, G. A.; Apitz, S. E. *Phys. Chem. Miner.* **1995**, *22*, 481.

(55) Smith, R. M.; Martell, A. E. *Critical Stability Constants*; Inorganic Complexes, Vol. 4; Plenum Press: New York, 1976.

(56) Huheey, J. E. *Inorganic Chemistry*, 3rd ed.; Harper and Row: New York, 1983.

(57) Rustad, J. R.; Dixon, D. A. Unpublished.